Research paper

Available Online at http://www.recentscientific.com

CODEN: IJRSFP (USA)

International Journal of Recent Scientific Research

International Journal of Recent Scientific Research
Vol. 17, Issue, 06, pp.736-744, June 2026

ISSN: 0976-3031

Subject Area : Physics

EXPLORING THIRD-ORDER NONLINEAR OPTICAL BEHAVIOR IN BIS[4-(2-AMINOETHYL) MORPHOLINE] CADMIUM DIACETATE TETRAHYDRATE SINGLE CRYSTALS

B. Chidambaranathan[1], P. Vijayamathubalan[1], S. Sivaraj[2], R. Gunaseelan[2], P. Sutharsan[3], S. Abraham Rajasekar[3*] and S. Selvakumar[1]

[1]PG and Research Department of Physics, Government Arts College (Autonomous), Chennai 600 035, Tamil Nadu, India
[2]Department of Physics, Pachaiyappa's College for Men, Kanchipuram, 631 501, Tamil Nadu, India
[3]Department of Physics, Sir Theagaraya College, Old Washermanpet, Chennai 600 021, Tamil Nadu, India

DOI: http://dx.doi.org/10.24327/ijrsr.20261706.0134

ARTICLE INFO

Article History:

Received 11th May 2026
Received in revised form 22nd May2026
Accepted 13th June 2026
Published online 28th June 2026

Key words:

Morpholine family crystal; FTIR; Z-scan; Thermal; Dielectric; Hardness.

ABSTRACT

A novel hybrid single crystal of bis[4-(2-aminoethyl) morpholine] cadmium diacetate tetrahydrate (AEMCA) with a bar-like transparent morphology was grown by the slow evaporation solution growth technique. The unit-cell parameters of AEMCA were determined as a = 8.8639(4) Å, b = 9.1035(5) Å, c = 9.2106(5) Å, α = 66.004(2)°, β = 73.603(2)°, γ = 70.161(2)°, and V = 629.63(6) Å³ by single-crystal X-ray diffraction analysis. FTIR analysis confirmed the presence of characteristic functional groups through molecular vibrations. The UV–Vis study revealed a cut-off wavelength of 260 nm and an optical band gap of 4.75 eV, highlighting its potential for optical applications. Z-scan analysis was used to evaluate nonlinear optical parameters such as the nonlinear refractive index (n_0), nonlinear absorption coefficient (β), and third-order nonlinear susceptibility (χ^3), which was found to be 2.148 × 10^{-7} esu. Interestingly, the χ^3 value of AEMCA is significantly higher than that of potassium dihydrogen phosphate (KDP). The crystal exhibits thermal stability up to 100 °C. Vickers microhardness measurements indicate that AEMCA belongs to the soft material category. The frequency-dependent electrical response of the sample was studied at room temperature.

INTRODUCTION

Attention has been exhibited to the crystal engineering of hybrid organic-inorganic materials because of their ability to frame supramolecular structures with the upgraded figure of merit to drive nonlinear optics from the laboratory to real-time applications [1 - 3]. Ionic salt materials provide an important and extremely flexible approach for the development of new materials that are applicable over a very broad range of frequencies [4]. The inclusion of an inorganic additive with an organic molecule provides high optical nonlinearity, chemical resilience, thermal stability and fabulous transmittance in the visible region [5 - 9]. Morpholine is a kind of secondary aliphatic amine. The addition of a suitable anion in the six-member ring makes the molecule a good nucleophile. In the development of novel nonlinear optical materials based on morpholine, an aliphatic ring can serve as an acceptor group. These compounds optical nonlinearities can be improved by enhancing the acceptor character of the aliphatic ring [10, 11]. Because of their propensity to take protons in the presence of acids, they have become an important component in nonlinear optical applications [12]. Morpholine and its derivatives, when combined with inorganic complexes, may form a sophisticated assembly from discrete ionic or molecular building pieces due to the strength and directionality of hydrogen bonds [13].

Protonated inorganic acids salts are an important class of nonlinear optical materials; interest has been increased after the discovery of promising nonlinear optical properties in molecular-ionic crystals of morpholinium nitrate [14], morpholinium perchlorate [15], morpholinium tetrafluoroborate [16] and morpholinium bromide [17]. The

*Corresponding author: **Dr. S. Abraham Rajasekar**

Associate Professor, Department of Physics,
Sir Theagaraya College, Old Washermanpet, Chennai 600 021, Tamil Nadu, India

technique of producing these materials has gained significant popularity due to their prospective uses. Ratajczak et al. [18] also reported on morpholinium dihydrogen phosphate's crystal structure, spectral properties and SHG efficiency. Morpholine is widely regarded as a useful ligand for the synthesis of a diverse spectrum of organometallic compounds [19, 20], including discrete complexes [21] and metal–organic polymers [22]. Although a morpholine molecule has the potential to be an ambidentate N - and O - donor ligand, morpholine is typically bound to a metal centre via the nitrogen atom [23, 24], unless the nitrogen atom is protonated [25, 26]. As a result, the oxygen atom can operate as a halogen-bond acceptor [27] or engage in hydrogen bonding [28], resulting in a wide range of supramolecular structures. In the O - halogen bond, the O atom works, while the halogen (except F) acts as a donor. The hydrogen atom of the secondary amino group can be easily replaced by an electrophilic species, allowing morpholine to be derivatized into matching hydrazine, carbonyl compounds or Schiff bases [29-32]. The carboxylation of the nitrogen atom, which produces morpholine-N-carboxylic acid or the corresponding morpholine-N-carboxylate (Morph COO^-) anion [33], is a potentially intriguing method of derivatizing the morpholine molecule. This should function as an anionic ligand, coordinating metal ions via the carboxylate group [34]. In the ongoing research on 4-(2- aminoethyl) morpholine, four new compounds were synthesized and reported their crystal structure by our group [35-38]. In this present work, a synthesized compound of bis[4-(2-aminoethyl) morpholine] cadmium diacetate tetrahydrate (AEMCA) was grown as a single crystal and its physiochemical properties such as spectral, optical, thermal, mechanical and electrical are discussed.

SYNTHESIS AND GROWTH OF AEMCA

According to the reaction strategy (Fig. 1), commercially available analytical grade (Merck, 99%) 4-(2-aminoethyl) morpholine (2 moles) and cadmium acetate dihydrate (1 mole) were combined in double deionized water. The recrystallization method enhanced the purity of the synthesized salt. The saturated solution was filtered and left to gently evaporate at ambient temperature (303 K). After 30 days, well-defined, clear, bar-shaped crystals with excellent morphology were extracted. Fig. 2 is an image of a grown single crystal of AEMCA measuring 7 x1 x 1 mm^3. Fig. 3 depicts the morphology of AEMCA.

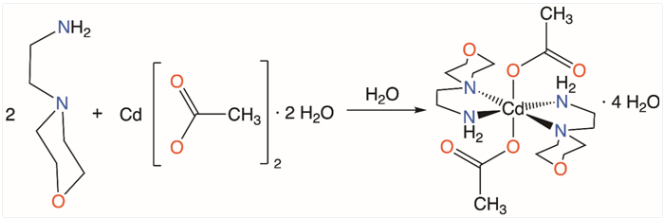

Fig. 1 Reaction scheme of AEMCA compound

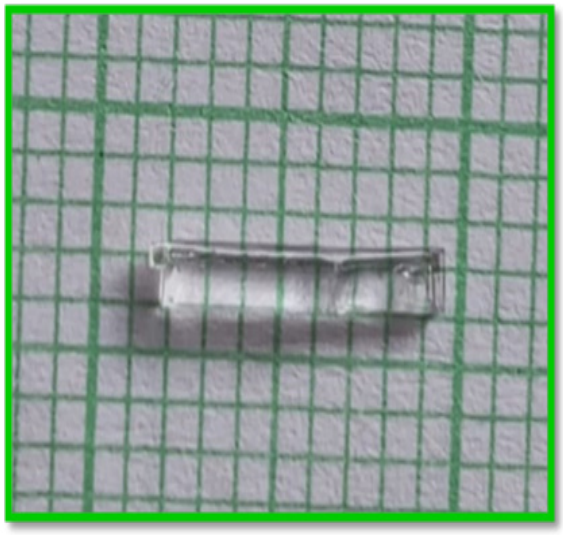

Fig. 2 Photograph of as-grown AEMCA single crystal

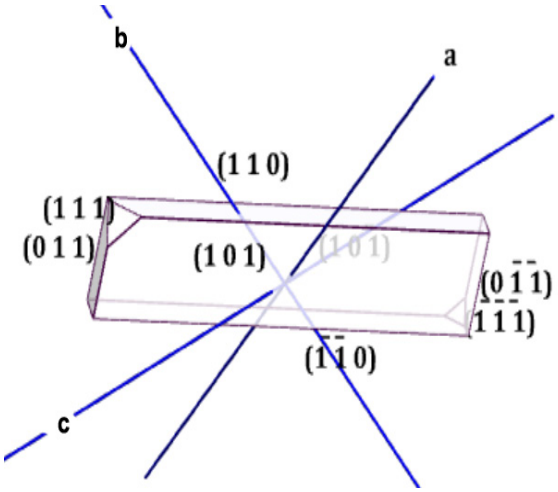

Fig. 3 Morphology of AEMCA single crystal

RESULTS AND DISCUSSION

Single crystal XRD analysis

To validate AEMCA complex production, a Bruker kappa APEX II diffractometer was used with graphite monochromatic Mo Kα radiation (λ=0.71073 Å) at 296 K. The intensity of X-ray data was measured for a grown AEMCA crystal. Table 1 summarises the derived unit cell parameter values. The complete structural data have been analysed and reported in our previous article [37].

Table 1. Crystal structure data of AEMCA

Crystal parameters	Data
Chemical formula	$[Cd(C_2H_3O_2)_2(C_6H_{14}N_2O)_2] \cdot 4H_2O$
Molecular weight (g/mol)	562.93
Crystal system, space group	Triclinic, P^{-1}
Temperature (K)	296
a, b, c (Å)	8.8639 (4), 9.1035 (5), 9.2106 (5)
α, β, γ ()	66.004 (2), 73.603 (2), 70.161 (2)
V ($Å^3$)	629.63 (6)
Z	1
Crystal size (mm)	0.42 x 0.25 x 0.20

FTIR study

The FTIR spectrum of AEMCA (Fig. 4) was recorded in the wavenumber range of 4000-400 cm^{-1} using Bruker FTIR spectrometer by KBr pellet technique. The ssignments are discussed in three different regions namely the high wavenumber region (3300-2000 cm^{-1}), medium wavenumber region (2000-1000 cm^{-1}) and a low wavenumber region (below 1000 cm^{-1}). In the high wavenumber region, there are four characteristic peaks at 3287, 3220, 2969 and 2869 cm^{-1}. The NH_2 asymmetric and symmetric stretching vibration of morpholine yielded peaks at 3287 and 3220 cm^{-1} but their feature is very much different from that observed for free morpholine [39]. In comparison to 4-(2-aminoethyl) morpholine (AEM), peak broadening is significantly enhanced in AEMCA which confirms the interaction between the acetate carbonyl group and NH_2 group in the coordination sphere. The CH_2 asymmetric and symmetric stretching vibrations are observed at 2969 and 2887 cm^{-1}, respectively. The NH_2 bending vibrations yielded a sharp peak at 1587 cm^{-1} and a shoulder peak at around 1628 cm^{-1}. is shifted to a very low wavenumber compared to that of free morpholine (AEM). The CH_3 and CH_2 bending vibrations are observed at 1440 cm^{-1} and 1363 cm^{-1}, respectively. The symmetric (C-O) vibration occurred at 1262 cm^{-1}. The bands observed at 1165 and 1101 cm^{-1} are asymmetric and symmetric vibrations of (C-O-C), respectively. The bands at 1065 and 849 cm^{-1} are due to symmetric stretching and bending vibrations of (C-O) and (C-H), respectively. The COO deformation occurs at 652 cm^{-1}. The band at 538 cm^{-1} is attributed to the metal coordination with the nitrogen of the morpholine ligand. The vibrational assignments are compared with the free morpholine ligand and summarized in Table 2.

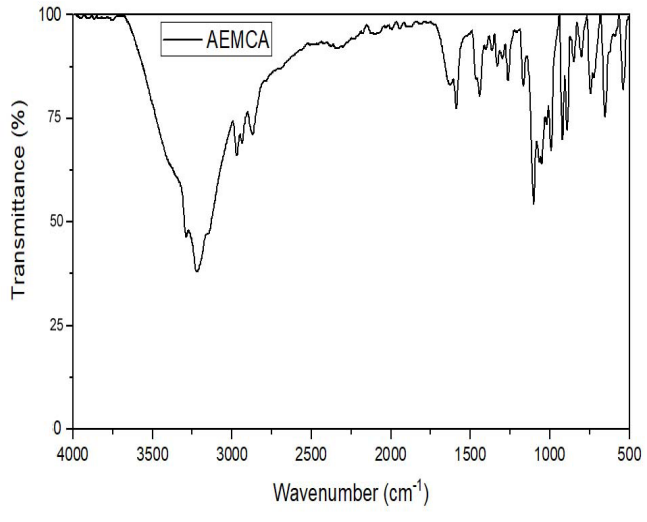

Fig. 4 FTIR spectrum of AEMCA

Table 2 Wavenumber assignments of AEMCA with 4-(2-aminoethyl) morpholine

Wavenumber (cm^{-1})		Assignment
4-(2-aminoethyl) morpholine	AEMCA	
3365	3287	γ_{as}(N-H)
-	3220	γ_{s} (N-H)
2864	2969	γ_{as}(CH_2)
-	2869	γ_{s} (CH_2)
1658	1628, 1587	δ (NH_2)
-	1440	δ (CH_3)
1355	1363	δ (CH_2)
1308	1328	γ_{s} (NH_2)
1273	1262	γ_{s} (C-O)
-	1165	γ_{as} (C-O-C)
1115	1101	γ_{s} (C-O-C)
1069	1065	γ_{s} (C-O)
866	849	δ (C-H)
764	742	γ_{s} (C-N)
-	652	COO deformation
-	538	(Cd-N)

γ_s - symmetric stretching; γ_{as} - asymmetric stretching; δ – bending

UV-Vis -NIR studies

The optical transmission range and the transparency cut-off wavelength play a vital role in the design of NLO materials. The UV-Vis-NIR spectrum of AEMCA crystal has been recorded in the wavelength region 200-1200 nm using a Perkin Elmer LAMBDA 950 Spectrophotometer. The UV-Vis-NIR absorption and transmission spectra of AEMCA crystals are shown in Fig. 5. The crystal exhibits 85–90% transmission over the wavelength range of 260–1200 nm. The cut-off rwavelength of AEMCA crystal was found to be 260 nm, which was attributed to the promotion of an electron from a 'non-bonding' (lone-pair) n orbital to a 'anti-bonding' π orbital designated as π* (n → π*) due to the bonding of cadmium acetate ion with the morpholinium cation. No characteristic absorption was observed in the entire visible region. The following Tauc's plot relation (Eq. 1) used to calculate the direct band gap energy:

$$\alpha h\upsilon = A\left(h\upsilon - E_g\right)^{\frac{1}{2}} \ldots\ldots\ldots (1)$$

where α is absorption coefficient, hυ represents photon energy and A is a constant. The crystal's band gap was calculated as 4.75 eV by graphing $(\alpha h\nu)^2$ against hν (Fig. 6). Based on the following equations (2 and 3), the linear refractive index (n_o) and extinction coefficient (K) of AEMCA are calculated [40 - 42]:

$$n_o = \frac{1}{T} + \left(\frac{1}{T} - 1\right)^{\frac{1}{2}} \quad \ldots\ldots\ldots (2)$$

$$K = \frac{\lambda\alpha}{4\pi} \quad \ldots\ldots\ldots\ldots (3)$$

Where T is the transmittance and $\boldsymbol{\lambda}$ is the wavelength. The extinction coefficient of a crystal is the percentage of light lost from scattering and absorption per unit distance in a medium. Figs. 7 and 8 show the computed extinction coefficient and refractive index as functions of wavelength. The low value of the refractive index indicates that the grown crystal is useful for anti-reflection coating in solar thermal devices.

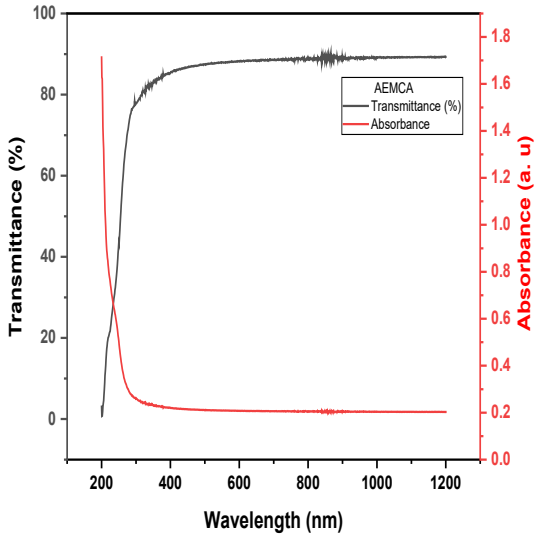

Fig. 5 Optical transmittance-absorbance of spectra of AEMCA

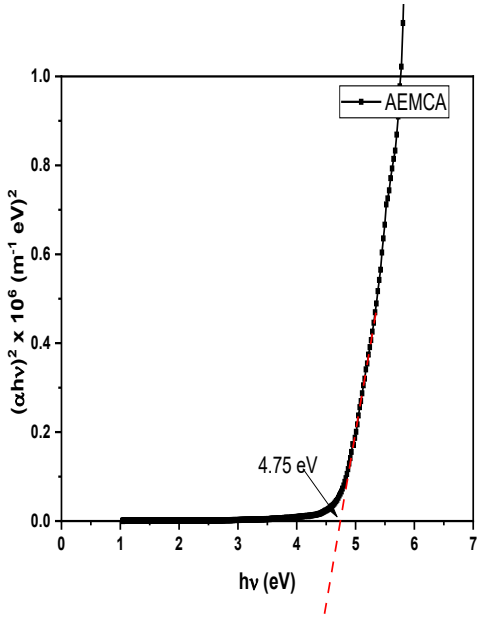

Fig. 6 Tauc's plot of AEMCA

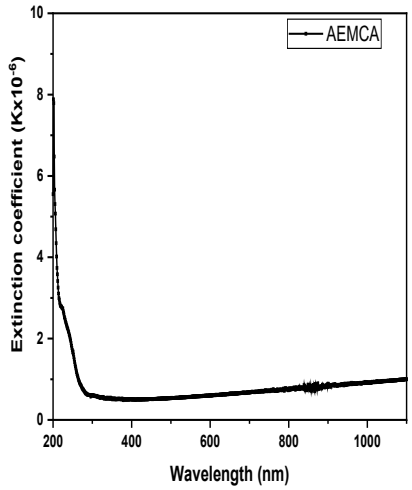

Fig. 7 Plot of extinction coefficient vs wavelength for the AEMCA

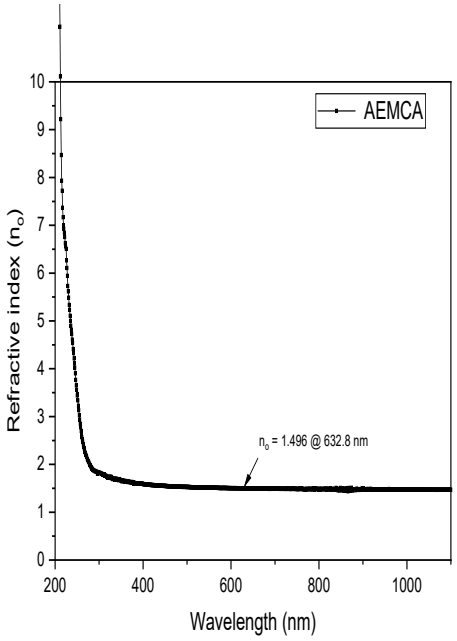

Fig. 8 Plot of the refractive index vs wavelength for the AEMCA

3.4. Z-scan study

The Z-scan experiment was carried out with a diode laser at 632.8 nm and a power of 12 mW. The beam waist was created by focusing the polarised Gaussian laser beam of mode TEM_{00} through a convex lens with a focal length of 20 cm. Typically, in Z-scan characterization approaches, the Z-scan curve displays normalized transmittance as a function of sample location Z relative to the focus plane. The Z-scan normalized transmittance is determined using the starting and steady-state values of the transmitted intensity in the AEMCA crystal as a function of sample location Z relative to the focus point. The magnitude and sign of the nonlinear refractive index, nonlinear absorption coefficient and third-order susceptibility are calculated using Z-scan data. Fig. 9 shows the difference between the prefocal transmittance maximum (peak) and postfocal transmittance lowest (valley) in the Z-scan curve, which yields the value of ΔT_{P-V}. According to the Fig. 9, the normalized transmittance peak followed by the valley indicates that the nonlinear refractive index is negative, resulting in the photorefractive lens effect (self-defocusing) [42]. The nonlinear refractive index (n_2) is -3.783x10^{-9} cm^2/W [43], as calculated using the Eq. 4. Eq. 5 yields the nonlinear absorption coefficient (β) of 2.385x10^{-4} cm/W, where ΔT represents the normalized transmittance with an open aperture (Fig. 10). It is seen that such Z-scan curves with no aperture are symmetric about the focus (Z=0), where they exhibit the highest transmittance (multiphoton absorption) [44, 45].

$$n_2 = \frac{\Delta\Phi_o}{k\, I_o\, L_{eff}} \quad cm^2/W \quad \ldots\ldots\ (4)$$

Heer, $k = \frac{2\pi}{\lambda}$

where k is a wavevector (9.9241x10^6 m^{-1}), and I_o is the laser beam intensity at the focal point (29.4 MW) and L_{eff} is the effective thickness (9.89x10^{-4} m).

$$\beta = \frac{2\sqrt{2}\Delta T}{I_o L_{eff}} \quad cm/W \quad \ldots\ldots \quad (5)$$

The real and imaginary parts of the third-order nonlinear optical susceptibility of the AEMCA were calculated by using the following equations (6 & 7). In that equation, c is the velocity of light ($3x10^8$ m/s) and ε_o is the permittivity of vacuum (8.854×10^{-12} F/m).

$$R_e\chi^{(3)}(esu) = \frac{10^{-4}\varepsilon_o c^2 n_2 n_o^2}{\pi}\left(\frac{cm^2}{W}\right) \quad \ldots\ldots\ldots \quad (6)$$

$$I_m\chi^{(3)}(esu) = \frac{10^{-2}\varepsilon_o c^2 n_o^2 \lambda\beta}{4\pi^2}\ (cm/W) \quad \ldots\ldots \quad (7)$$

$$\chi^{(3)} = \sqrt{(R_e\chi^{(3)})^2 + (I_m\chi^{(3)})^2} \quad \ldots\ldots \quad (8)$$

According to the Eq. 8, third-order susceptibility of the AEMCA crystal is $2.148x10^{-7}$ esu, which is significantly higher than those of other well-known nonlinear optical crystals such as KDP ($8.34x10^{-14}$ esu), BBO ($5.7x10^{-14}$ esu) and $LiNbO_3$ ($33.7x10^{-14}$ esu) [46, 47]. The calculated linear and nonlinear optical parameters of the AEMCA crystal are presented in Table 3.

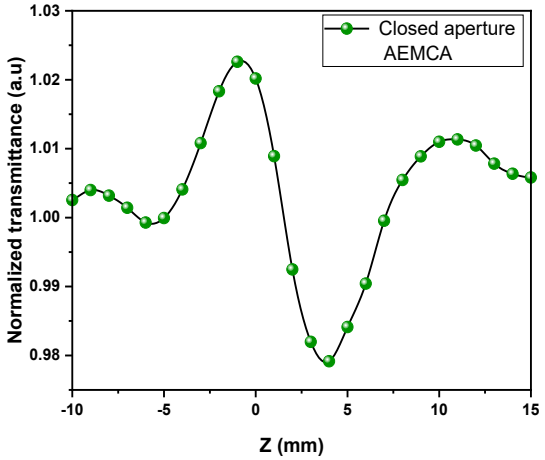

Fig. 9 Closed aperture spectrum of the AEMCA

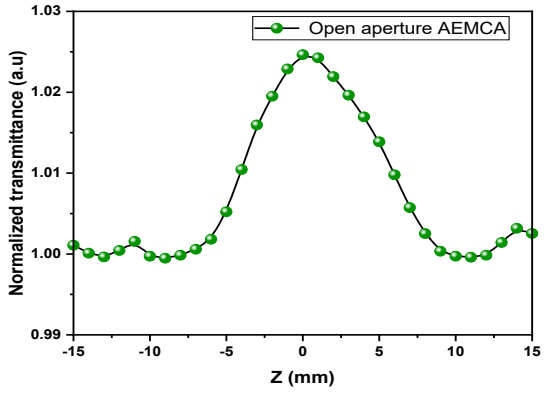

Fig. 10 Open aperture spectrum of the AEMCA

Table 3 Linear and nonlinear optical parameters of AEMCA

Parameters	Calculated values
Laser beam wavelength (λ)	633 nm
Focal length of the lens (f)	20 cm
Power of the laser (P)	12 mW
Diameter of the laser beam (d)	5 mm
Beam radius at the aperture (W_a)	9 mm
Radius of aperture (r_a)	2 mm
Linear absorption coefficient (α)	12.4 m^{-1}
Linear refractive index (n_o)	1.496
The difference between the peak and valley	
transmission (ΔT_{p-v}) from Figure 9.	0.04346
The difference between the maximum transmittance	
and valley peak (ΔT) from Figure 10.	0.02464
Nonlinear refractive index (n_2)	$-3.7833x10^{-9}$ cm^2/W
Nonlinear absorption coefficient (β)	$2.38483x10^{-4}$ cm/W
Real part of the third-order susceptibility (Re (χ^3))	$-2.15x10^{-7}$ esu
Imaginary part of the third-order susceptibility (Im (χ^3))	$6.82x10^{-8}$esu
Third order nonlinear susceptibility (χ^3)	$2.148x10^{-7}$ esu

3.5. Thermal studies

The thermal study of AEMCA was performed using a NETZCH STA 2500 thermal analyzer. The starting weight of 13.09 mg was used to record TGA and DTG traces at temperatures ranging from 27 to 1000 °C, with a nitrogen environment and a heating rate of 10 K/min maintained. Alumina was used as the reference material in an Al_2O_3 crucible. Figure 11 shows AEMCA's thermogravimetric (TG) and derivative thermogravimetric (DTG) thermograms. The TG–DTG curves reveal a multistep decomposition process with distinct mass-loss events. Initially, the crystal exhibits negligible weight loss up to approximately 80 °C, indicating the absence of loosely bound surface moisture and confirming the good thermal stability of the material at ambient conditions. The first decomposition stage occurs between 80 and 150 °C, accompanied by a DTG peak centered at 118.7 °C. This mass loss is attributed to the release of four lattice water molecules present in the crystal structure. The second decomposition stage is observed in the temperature range of approximately 150 – 240 °C, with a DTG maximum at 193.4 °C. This stage corresponds to the partial decomposition of coordinated organic moieties, primarily involving the acetate groups and the initial breakdown of the 4-(2-aminoethyl)morpholine ligands. A major and rapid decomposition event occurs between 240 and 300 °C, as evidenced by the intense DTG peak at 287.9 °C. This stage is associated with the complete degradation of the organic ligands and acetate groups, resulting in a substantial mass loss. The TG curve shows a sharp decrease in mass from about 55 – 60% to nearly 23%, indicating the collapse of the organic framework surrounding the cadmium center. Beyond 300 °C, the decomposition proceeds gradually with minor

mass-loss steps extending up to 1000 °C. These processes are attributed to the oxidation and carbonization of residual organic fragments, producing volatile gases such as CO_2, CO, NH_3, and other decomposition products. The gradual decline in mass suggests the formation of thermally stable inorganic residues. At temperatures above 700 °C, the TG curve reaches a relatively stable region, leaving a final residue of approximately 7 – 10 wt.% at 1000 °C. This residue is likely composed of cadmium-containing inorganic species, predominantly CdO formed through the thermal oxidation of cadmium-containing intermediates. The absence of any significant decomposition below approximately 100 °C and the major decomposition onset above 150 °C indicate that the AEMCA crystal possesses moderate thermal stability.

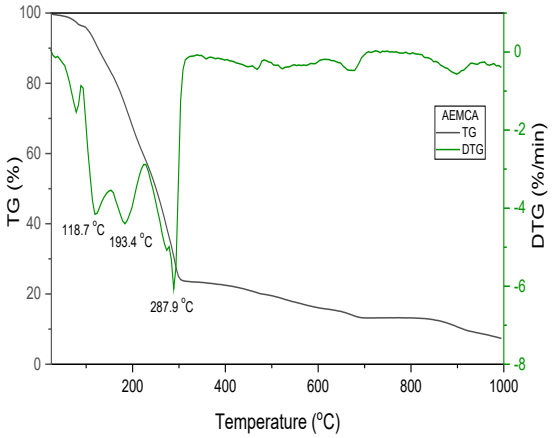

Fig. 11 TG – DTG traces of AEMCA

Microhardness study

The indentation diagonal length (d) was measured for various loads (P) of 25, 50, and 100 g on the (1 0 1) plane of AEMCA crystal with a fixed indentation time of 5 seconds using a Vicker's hardness indenter. Cracks formed on the crystal surface around the indenter when a 100 g indentation stress was applied. As a result, the experiment was not extended to include more loads. Cracks on the crystal surface occur as a result of the local release of internal stress caused by indentation. The Vicker's hardness number (H_v) was determined using Eq. 9.

$$H_v = 1.8544 \times \frac{P}{d^2} \ (kg/mm^2) \ \ldots\ldots\ldots (9)$$

Where, P is the load being applied (kilogram), and d is the indentation's diagonal length (millimetres).

Fig. 12 depicts how hardness numbers vary with applied loads. The figure shows that the hardness values rise with the load up to 100 g and attain 133 kg/mm^2. The developed crystal's work hardening coefficient value (n) was estimated using the least square fit approach on a plot of log P vs log d (Fig.13). The AEMCA crystal falls under the soft category of materials, as indicated by the measured work-hardening coefficient of 6.023 [48].

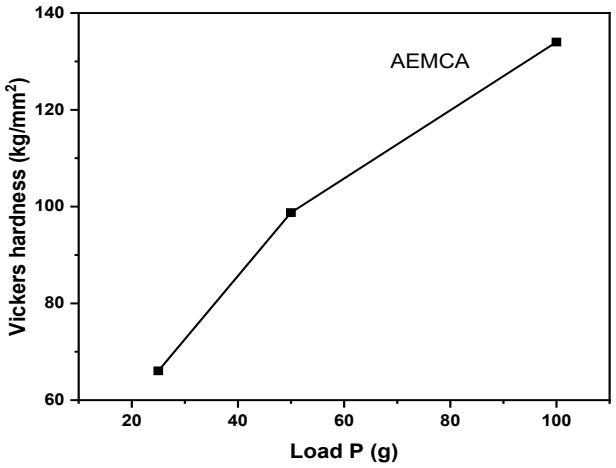

Fig. 12 Variation of H_V with applied load P for AEMCA

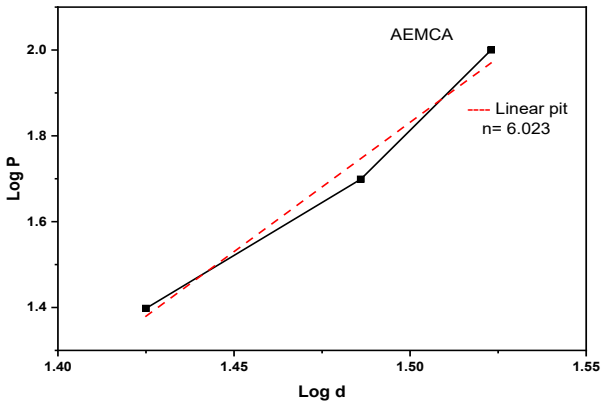

Fig. 13 Plot of log d versus log P for AEMCA

3.7. Dielectric Study

The dielectric constant and dielectric loss were measured on the (1 0 0) plane of an AEMCA crystal as a function of frequency between 100 Hz and 5 MHz at room temperature (303 K) with a HIOKI LCR METRE 1M3536. The crystal was painted with silver on the parallel faces of (1 0 0) planes to achieve ohmic contact with the electrodes. Figures 14 and 15 show how dielectric constant and dielectric loss change with log frequency. The plot (Fig. 14) demonstrates that the dielectric constant deteriorates rapidly from 127 to 35 as frequency increases from 100 Hz to 4 kHz, eventually nearing a constant value of 30. This could be related to the effects of space charge polarization. Furthermore, space charge polarization is determined by the material's purity and perfection. Figure 14 shows the same trend, with the dielectric loss decreasing with increasing frequency until it reaches an extremely low dielectric loss of 0.901 after 4 kHz. The reduced dielectric loss at high frequencies suggests that the crystal contains fewer flaws. Fig. 16 demonstrates the frequency-dependent variation in AC electrical conductivity. AC conductivity is low at low frequencies and increases with frequency. At low frequencies, the AC conductivity is due to certain carriers becoming trapped at the crystal's defect sites. The increase in AC conductivity may be due to a reduction in space charge polarization and cation disordering between adjacent locations [49].

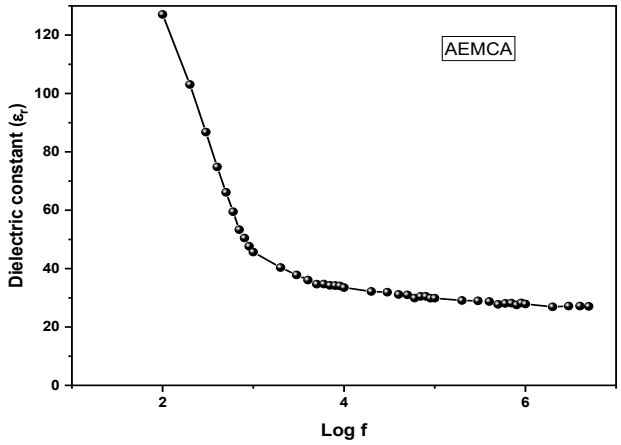

Fig. 14 Variation of dielectric constant as a function of frequency for AEMCA

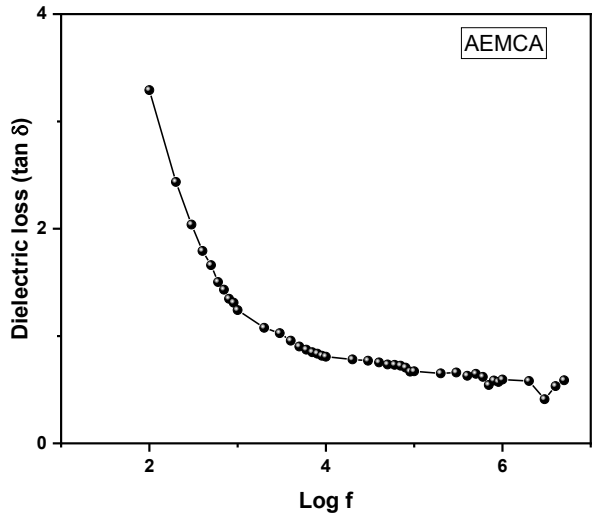

Fig. 15 Variation of dielectric loss as a function of frequency for AEMCA

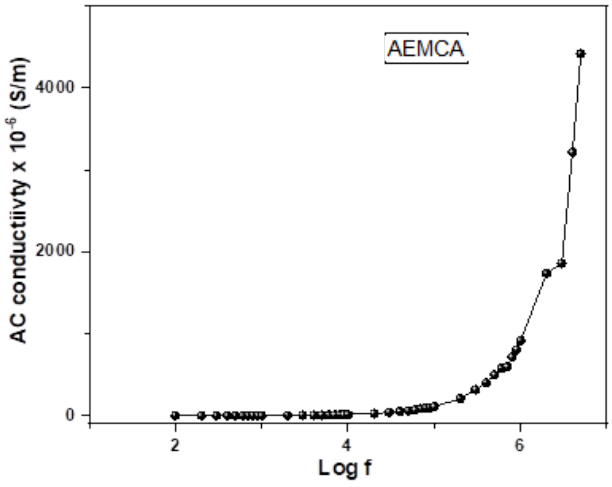

Fig. 16 Variation of AC conductivity as a function of frequency for AEMCA

CONCLUSION

Single crystals of AEMCA were produced using a slow evaporation approach. Single-crystal XRD analysis confirms the structure of produced crystals. It also displays the supramolecular structure, Hirsfeld surfaces, and hydrogen bond interactions. The FTIR spectrum reveals the functional frequencies of AEMCA molecules. This crystal's transmission spectrum displays a large transmission window, with 85 - 90 percent transmittance across the visible area. The optical band gap was determined to be 4.75 eV. Z-scan measurements were performed using a diode laser at 633 nm, and the third-order susceptibility was determined to be 2.148×10^{-7} esu. Closed aperture z-scan reveals that the peak-valley fluctuation is due to the self-defocusing effect of the AEMCA, which indicates the negative nonlinear refraction and the value obtained is -3.78325×10^{-9} cm^2/W. The thermal investigation using the TG-DTG technique shows that the AEMCA is thermally stable up to 100 °C crystal. Microhardness investigations on AEMCA crystal demonstrate that when the load increases, the microhardness number drops, indicating that the material is soft. At low frequencies, the dielectric constant and dielectric loss are significant, whereas at high frequencies they are low. The combined optical, electrical, and structural characteristics establish AEMCA as a potential candidate for advanced nonlinear optical and high-frequency electronic applications.

Acknowledgment

The authors are thankful to SAIF, IIT-Madras, for single-crystal XRD analysis, SSN College of Engineering, Chennai, for the Z-SCAN study, and Archbishop Casimir Instrumentation Centre (ACIC), St. Joseph College (Autonomous), Tiruchirappalli, for providing FTIR, UV-visible and Hardness studies.

Author Contributions

All authors contributed to the study's conception and design. Materials preparation and analyses were performed by all the authors. All authors read and approved the final manuscript.

Competing Interests

The authors declare that they have no known competing financial interests or personal relationships that could have appeared to influence the work reported in this paper.

Research Data Policy and Data Availability Statements

All data generated or analyzed during this study are included in this manuscript.

References

1. R. W. Munn, C. N. Iron side, Principles and Applications of Nonlinear Optical Materials, Chapman and Hall, London, (1993). https://doi.org/10.1007/s10854-016-6171-0.
2. S. Selvakumar, S. M. Ravi Kumar, K. Rajarajan, A. Joseph Arul Pragasam, S. A. Rajasekar, K. Thamizharasan, and P. Sagayaraj, Crystal Growth & Design, 6, 10 (2006) 2607-2610. https://doi.org/10.1021/cg060414p.
3. K. Rajarajan, G. Mani, I. Vetha Potheher, Joe G. M. Jesudurai, M. Vimalan, Dennis Christy, J. Madhavan and P. Sagayaraj, Journal of Physics and Chemistry of Solids, 68 (2007) 2370–2375. doi:10.1016/j.jpcs.2007.07.036.

4. S. R. Marder, J. W. Perry and W. P. Schaefer, J. Mater. Chem. 2 (1992). https://doi.org/10.1039/JM9920200985.
5. D. Eimerl, S. Velsko, L. Davis, F. Wang, G. Loiacono, and G. Kennedy, IEEE J. Of Quantum Electronics. 25, 179-193 (1989). https://doi.org/10.1109/3.16261.
6. S. Selvakumar, S. M Ravi Kumar, Ginson P. Joseph, K Rajarajan, J. Madhavan, S. A. Rajasekar and P Sagayaraj, Journal of Materials Chemistry and Physics, 103 (2007) 153-157. https://doi.org/10.1016/j.matchemphys.2007.02.005.
7. S. A. Rajasekar, K. Thamizharasan, A. Joseph Arul Pragasam, J. Packiam Julius and P. Sagayaraj, Journal of Crystal Growth, 247 (2003) 199–206. https://doi.org/10.1016/S0022-0248(02)01977-2.
8. Reena Ittyachan and P. Sagayaraj, Journal of Crystal Growth, 249 (2003) 553–556. https://doi.org/10.1016/S0022-0248(02)02115-2.
9. A. Joseph Arul Pragasam, S. Selvakumar, K. Thamizharasan, D. Prem Anand and P. Sagayaraj, Journal of Crystal Growth, 280 (2005) 271–278. doi:10.1016/j.jcrysgro.2005.03.057.
10. A. Parkin, Iain, D. H. Oswald and S. Parsons, Acta Crystallogr., Sec. B: Struct. 60, 219-227 (2004). http://dx.doi.org/10.1107/S0108768104003672.
11. I. Majerz, E. Kwiatkowska and A. Koll, J. Mol. Struct., 831, 106 – 113 (2007). https://doi.org/10.1016/j.molstruc.2006.07.029.
12. M. S. Girigoriev, E. E. German and A. Y. Maruk, Acta Crystallogr. Sec. E: Struct.. 64, o390-o403 (2008). https://doi.org/10.1107/S1600536807068134.
13. M. Owczarek, R. Jakubas, G. Bator, A. Pawlukojc, J. Baran, J. Przeslawskh and W. Medycki, Chemical Physics, 381, 11-2 (2011). https://doi.org/10.1016/j.chemphys.2011.01.002.
14. S. Swaminathan, and G.S. Murthy, Morpholinium nitrate, Acta Crystallogr., Sect. B: Struct., B32, 3140-3142, (1976). https://doi.org/10.1107/S0567740876009795.
15. A. Arunkumar and P. Ramasamy, J. Cryst. Growth, 388, 124-131 (2014). https://doi.org/10.1016/j.jcrysgro.2013.10.005.
16. P. Szklarz, M. Owczarek, G. Bator, T. Lis, K. Gatner and K. Jakubas, J. Mol. Struct., 929, 48-57 (2009). https://doi.org/10.1016/j.molstruc.2009.04.014.
17. Kamentherem Padayachy, Z. Mgcima, M. A. Fernandes, H. M. Marques and A. S. Desousa, Acta Crystallogr. Sect. E: Struct. 67, o2594-o2601 (2011). https://doi.org/10.1107/S1600536811035598.
18. H. Ratajczak, J. Baran, J. Barycki, S. Deburs, M. May, A. Pietraszko, H.M. Ratajczak, A. Tramer and J. Venturini, J. Mol. Struct. 555, 149-158 (2000). https://doi.org/10.1016/S0022-2860(00)00596-2.
19. M. Beller, H. Trauthwein, M. Eichberger, C. Breindl, C. and Muller, T. E., Eur. J. Inorg. Chem. 7, 1121–1132 (1999).
20. https://doi.org/10.1002/(SICI)1099-0682(199907)1999:7%3C1121::AID-EJIC1121%3E3.0.CO;2-8.
21. M. Beller, H. Trauthwein, M. Eichberger, C. Breindl, C., Herwig and J. Muller, T. E. and Thiel, O. R., Eur. J. Inorg. Chem. 5, 1306–1319 (1999). https://doi.org/10.1002/(SICI)1521-3765(19990401)5:4%3C1306::AID-CHEM1306%3E3.0.CO;2-4
22. V. Stilinovic, K. Uzarevic, I. Cvrtila and B. Kaitner, CrystEngComm., 14, 7493–7501(2012). https://doi.org/10.1039/C2CE25848J.
23. H. Sil Moon, C. H. Kim and S. G. Lee, Bull. Korean Chem. Soc. 21, 339–341 (2000). https://doi.org/10.5012/bkcs.2000.21.3.339.
24. I. Cvrtila, V. Stilinovic, and B. Kaitner, Struct. Chem. 23 587–594 (2012). https://doi.org/10.1007/s11224-011-9905-x.
25. M. Cindric, G. Pavlovic, T. Hrenar, M. Uzelac and M. Curic, Eur. J. Inorg. Chem. 2013, 563–571(2013). https://doi.org/10.1002/ejic.201201050.
26. H. H. Li, Z. R. Chen, L. C. Cheng, Y. J. Wang, M. Feng and M. Wang, Dalton Trans. 39, 11000–11007 (2010). https://doi.org/10.1039/C0DT00622J.
27. R. D. Willett, R. Butcher, C. P. Landee, and B. Twamley, Polyhedron, 24, 2222–2231(2005). https://doi.org/10.1016/j.poly.2005.03.121.
28. G. Lapadula, N. Judas, T. Friscic and W. Jones, Chem. Eur. J., 16, 7400–7403 (2010). https://doi.org/10.1002/chem.201000049.
29. P. Weinberger, R. Schamschule, K. Mereiter, L. Dlhan, R. Boca, and W. Linert, J. Mol. Struct. 446, 115–126 (1998). https://doi.org/10.1016/S0022-2860(98)00280-4.
30. A. L. Johnson, N. Hollingsworth, A. Kingsley, G. Kociok Kohn and C. Molloy, Organometallics, 28, 2650–2653 (2009). https://doi.org/10.1021/om900121z.
31. C. Cheadle, J. Ratcliff, M. Berezin, V. Palshin, V. N. Nemykin, N. N. Gerasimchuk, Dalton Trans. 46, 13562–13581 (2017). https://doi.org/10.1039/C7DT02317K.
32. M. Tazi, W. Erb, Y. S. Halauko, O. A. Ivashkevich, V. E. Matulis, T. Roisnel, V. Dorcet and F. Mongin, Organometallics, 36, 4770 – 4778 (2017). https://doi.org/10.1021/acs.organomet.7b00659.
33. J. Hellmann, I. Rhotert, H. Westenberg, R. Frohlich, B. Wibbeling, W. Uhl and E. U. Wurthwein, Eur. J. Org. Chem. 16, 3356–3368 (2013). https://doi.org/10.1002/ejoc.201300208.
34. C. J. Brown and L. R. Gray, Acta Cryst. A 37 1981 C202. doi:10.1107/S0108767381093549.
35. C. N. R. Rao, S. Natarajan, and R. Vaidhyanathan, Angew. Chem. Int. Ed. 43 2004 466–496. https://doi.org/10.1002/anie.200300588.
36. B. Chidambaranathan, S. Sivaraj and S. Selvakumar, Acta Cryst. E79, 8-13 (2023). https://doi.org/10.1107/S2056989022011409
37. B. Chidambaranathan, S. Sivaraj, P. Vijayamathubalan and S. Selvakumar, Acta Cryst. E79, 226-230 (2023). https://doi.org/10.1107/S2056989023001470

38. B. Chidambaranathan, S. Sivaraj, P. Vijayamathubalan and S. Selvakumar, Acta Cryst. E79, 1049-1052 (2023). https://doi.org/10.1107/S2056989023008782
39. B. Chidambaranathan, S. Sivaraj, P. Vijayamathubalan, S. Abraham Rajasekar and S. Selvakumar, Acta Cryst., E80, 271-276 (2024). https://doi.org/10.1107/S2056989024000963
40. Bismi Edwin, M. Amalanathan, Ridhima Chadha, Nandita Maiti, Sudhir Kapoor and Hubert Joe, J. Mol. Struct. 1148, 459–470 (2017). https://doi.org/10.1016/j.molstruc.2017.07.075.
41. J. H. Joshi, S. Kalainathan, D. K. Kanchan, M. J. Joshi and K. D. Parikh, Arabian Journal of Chemistry, 13 (2020) 1532–1550. https://doi.org/10.1016/j.arabjc.2017.12.005.
42. Allen Moses S. E., Tamilselvan S., Ravikumar S. M., Vinitha G., Hegde T A., Shanmuga Sundar G. J., Vimalan M and Sivaraj S., J. Mater. Sci.: Mater. Electron, 30 (2019b) 9003–9014. https://doi.org/10.1007/s10854-019-01229-9.
43. S. Sivaraj, P. Vijayamathubalan, B. Chidambaranathan, R. P. Sagayaraj P and S. Selvakumar, Journal of Molecular Structure, 1324 (2025) 140705. https://doi.org/10.1016/j.molstruc.2024.140705.
44. Uma J. and Rajendran V., Progress in Natural Science: Materials International, 26 (2016) 24-31. http://dx.doi.org/10.1016/j.pnsc.2016.01.013.
45. Karuppasamy P., Muthu Senthil Pandian and Ramasamy P., J. Cryst. Growth, 473 (2017) 39–54. https://doi.org/10.1016/j.jcrysgro.2017.05.018.
46. S. Sivaraj, B. Chidambaranathan, P. Vijayamathubalan, R. Gunaseelan, P. Karuppasamy, P. Sagayaraj, S. Selvakumar, Journal of Molecular Structure, 1337 (2025) 142117. https://doi.org/10.1016/j.molstruc.2025.142117.
47. D. Wang, T. Li, S. Wang, J. Wang, Z. Wang, X. Xu and F. Zhang, RSC Adv., 6, 14490-14495 (2006). https://doi.org/10.1039/C5RA24761F.
48. M. Yin, H. P. Li, S. H. Tang, W. Ji, Appl. Phys. B70 587-591 (2000). https://doi.org/10.1007/s003400050866.
49. Onitsch E. M., Mikroskopie, Vol. 95 (1956) 12-14.
50. B. N. Parida, P. R. Das, R. Padhee and R. N. P. Choudhary, Adv. Mat. Lett., 3(3) 231-238 (2012). http://dx.doi.org/10.5185/amlett.2012.2321.

How to cite this article:

Chidambaranathan et al. (2026). Exploring third-order nonlinear optical behavior in bis[4-(2-aminoethyl) morpholine] cadmium diacetate tetrahydrate single crystals . *Int J Recent Sci Res*.17(06), pp.736-744.

****